

# Proximity induced time-reversal topological superconductivity in $\text{Bi}_2\text{Se}_3$ films without phase tuning

Oscar E. Casas,<sup>1,2</sup> Liliana Arrachea,<sup>3</sup> William J. Herrera,<sup>1</sup> and Alfredo Levy Yeyati<sup>2</sup>

<sup>1</sup>*Departamento de Física, Universidad Nacional de Colombia, Bogotá, Colombia*

<sup>2</sup>*Departamento de Física Teórica de la Materia Condensada C-V,*

*Condensed Matter Physics Center (IFIMAC) and Instituto Nicolás Cabrera, Universidad Autónoma de Madrid, E-28049 Madrid, Spain*

<sup>3</sup>*International Center for Advanced Studies, Escuela de Ciencia y Tecnología, Universidad Nacional de San Martín-UNSAM, Av 25 de Mayo y Francia, 1650 Buenos Aires, Argentina*

(Dated: January 14, 2022)

Many proposals to generate a time-reversal invariant topological superconducting phase are based on imposing a  $\pi$  phase difference between the superconducting leads proximitizing a nanostructure. We show that this phase can be induced on a thin film of a topological insulator like  $\text{Bi}_2\text{Se}_3$  in proximity to a *single* s-wave superconductor. In our analysis we take into account the parity degree of freedom of the electronic states which is not included in effective Dirac-like surface theories. We find that the topological phase can be reached when the induced interparity pairing dominates over the intraparity one. Application of an electric field perpendicular to the film extends the range of parameters where the topological phase occurs.

## I. INTRODUCTION

The interest in topological phases of matter and, in particular, in topological superconductors (TSs) has not ceased to grow [1]. In addition to their fundamental interest, TSs are predicted to host topologically protected Majorana zero modes (MZM) at the edges with potential applications in future quantum technologies [2].

Although topological superconductivity is expected to occur spontaneously in certain compounds like  $\text{Sr}_2\text{RuO}_4$  [3]; actual vigorous experimental progress is coming from the side of artificial nanostructures. In particular, clear signatures of MZMs have been demonstrated in hybrid nanostructures combining semiconducting nanowires with strong spin orbit (like InAs or InSb) and conventional superconductors [4–8].

As in the case of other proposals based on arrays of magnetic impurities [9] these platforms constitute a realization of broken-time reversal (symmetry class D) 1D topological superconductivity. Although the time-reversal counterpart or class DIII superconductivity has attracted great theoretical interest [10], its actual realization is still an experimental challenge. The zero energy excitations in this class of TSs are Kramers pairs of Majorana modes. While their braiding properties appear to be path dependent [11, 12], they exhibit other exotic transport [13, 14] and spin [4, 16–18] properties which render them objects of fundamental interest.

Intrinsic DIII superconductivity in two and three dimensional systems has been discussed in the literature (see for instance Refs. [19–21]) but also in this case most theoretical proposals have been focused on proximitized nanostructures. These, in general, require two basic ingredients: a multichannel or multiband electronic structure and a mechanism for inducing opposite pairing amplitudes on these channels [22]. These include Rashba nanowires proximitized by a d-wave [23] or an Iron-based

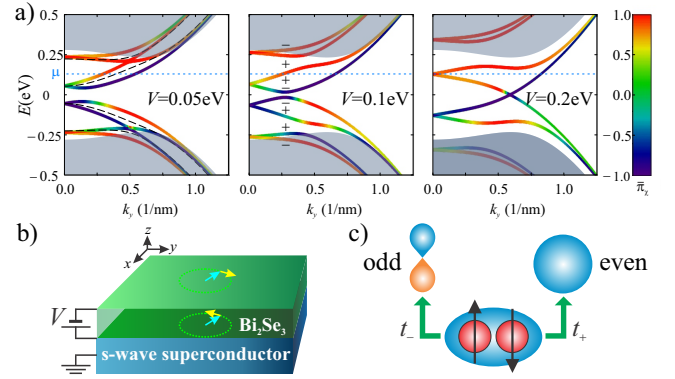


Figure 1: a) Surface states bands in a thin  $\text{Bi}_2\text{Se}_3$  film in the presence of an electric field, controlled by the biasing potential  $V$  between the top and bottom surfaces. The bands are helicity degenerate for  $V = 0$  (dashed lines in left panel) but the degeneracy is broken for finite  $V$ . The signs in the middle panel indicate the bands helicity and the color scale of the lines is set by the normalized relative weight,  $\bar{\pi}_\chi$ , of the surface states on the two parity sectors (with  $\bar{\pi}_\chi = 2\pi_\chi/(1+\pi_\chi^2)$ , where  $\pi_\chi$  is the relative weight defined in the main text). The gray areas indicate the regions for the bulk states and the dashed horizontal line indicates the position of the chemical potential. b) Geometry considered for analyzing the proximity effect. c) Schematic representation of the interparity pairing which can be induced from the s-wave superconductor.

superconductor with  $s_\pm$  pairing symmetry [24]; or two parallel nanowires with interwire pairing [25–27] or subject to opposite Zeeman fields [28]. Another scenario is spin orbit and many body interactions in proximity with ordinary superconductivity [29, 30]. Induction of the DIII phase on the edge or surface states of a 2D or a 3D topological insulator (TI) has also been considered [26, 31–35]. Refs. [33, 35] suggest that for the case of a

thin 3D TI film reaching the DIII phase requires forming a S/TI/S junction and imposing a  $\pi$ -phase difference. These studies are based on effective 2D models describing the surface states on the 3D TI film.

In the present work we propose a new approach for the case of proximitized 3DTI thin films. In contrast to previous works which start from the projected 2D theory, we use a 3D model which keeps track of the parity degree of freedom. We show that the DIII-TS phase may arise naturally by proximity to a *single* s-wave superconductor when considering the presence of interparity pairing. We further show that the inclusion of an external electric field, breaking inversion symmetry, helps to stabilize this topological phase.

The main ingredients of the proposed mechanism are illustrated in Fig. 1. The surface states of a 3D TI are characterized by a well defined helicity, i.e. they are eigenstates of the helicity operator  $\hat{h} = (\boldsymbol{\sigma} \times \mathbf{k}_{\parallel})_z / k_{\parallel}$ , where  $\mathbf{k}_{\parallel}$  is the wave vector parallel to the surface and  $\sigma_{\alpha}$  are Pauli matrices in spin space [1]. In addition, these states are also characterized by a certain parity pseudospin, which depends on the surface orientation and on the material. For instance, in films of the  $\text{Bi}_2\text{Se}_3$  family grown along the  $c$  axis, states on opposite surfaces have opposite helicities and opposite parity pseudospin [37]. In sufficiently thin films, the surface states corresponding to opposite sides are not fully decoupled but hybridize to some extent [38, 39] and the helicity degeneracy can be broken by an electric field perpendicular to the film, as illustrated in Fig. 1(a). Therefore, when one of the surfaces is in contact with a superconductor as in Fig. 1(b), superconductivity is induced into the two surfaces in both parity channels, as well as interparity, as schematically depicted in Fig. 1(c). Interestingly, the interparity component induced on each helical channel typically have opposite signs. Our goal is to show that for the case of an s-wave superconductor, the TS phase can be reached provided that the interparity component is large enough and inversion symmetry is broken.

## II. MODEL FOR A TI FILM AND PROXIMITY EFFECT

The low energy and long wavelength electronic properties of a TI of the  $\text{Bi}_2\text{Se}_3$  family can be described by the  $\mathbf{k}\cdot\mathbf{p}$  Hamiltonian introduced in Ref. [1] in a basis of four states which are combinations of  $p_z$  orbitals on the Bi and Se sites with even and odd parities. For analyzing the proximity effect it is convenient to perform a unitary transformation [2, 37] with respect to the model in Ref. [1] [see discussion in the Supplementary Material (SM), Ref. 41], which yields

$$H^{3D} = \mathcal{M}(\mathbf{k})\tau_z \otimes \sigma_0 + A_1 k_z (\tau_y \otimes \sigma_0) - A_2 [k_x (\tau_x \otimes \sigma_y) - k_y (\tau_x \otimes \sigma_x)], \quad (1)$$

where  $\mathcal{M}(\mathbf{k}) = M_0 - B_1 k_z^2 - B_2 (k_x^2 + k_y^2)$  [42], while  $\tau_{\alpha}$  are Pauli matrices operating in parity space. This Hamiltonian

commutes with the helicity operator, leading to the properties of the surface states commented above.

In order to describe the proximitized thin film we now switch into a tight-binding (TB) description of the electronic structure. For this purpose we follow Ref. [43] and introduce a cubic lattice with parameter  $a \sim 1$  nm oriented along the  $c$ -axis and consider the  $\mathbf{k}\cdot\mathbf{p}$  Hamiltonian as a long-wavelength expansion of this TB model. We shall consider the case of films of thickness  $L_z = N_z a$  and impose periodic boundary conditions on the  $x, y$  directions. In the basis  $\psi_{k_{\parallel}, i} = (c_{k_{\parallel}, i+\uparrow}, c_{k_{\parallel}, i+\downarrow}, c_{k_{\parallel}, i-\uparrow}, c_{k_{\parallel}, i-\downarrow})^T$ , where  $c_{k_{\parallel}, i\tau\sigma}^{\dagger}$  creates an electron with parallel momentum  $\mathbf{k}_{\parallel}$  on the  $i$ -layer within the film, parity  $\tau$  and spin  $\sigma$ . The TB model adopts the form  $\hat{H}^{TB} = \sum_{k_{\parallel}, ij} \psi_{k_{\parallel}, i}^{\dagger} \hat{\mathcal{H}}(\mathbf{k}_{\parallel})_{ij} \psi_{k_{\parallel}, j}$  where

$$\begin{aligned} \hat{\mathcal{H}}(\mathbf{k}_{\parallel})_{ij} = & \epsilon(\mathbf{k}_{\parallel}) (\tau_z \otimes \sigma_0) \delta_{ij} + \frac{A_2}{a} [\sin k_y a (\tau_x \otimes \sigma_x) \\ & - \sin k_x a (\tau_x \otimes \sigma_y)] \delta_{ij} + \frac{B_1}{a^2} (\tau_z \otimes \sigma_0) (\delta_{ij-1} + \delta_{ij+1}) \\ & - \frac{iA_1}{2a} (\tau_y \otimes \sigma_0) (\delta_{ij-1} - \delta_{ij+1}), \end{aligned} \quad (2)$$

with  $\epsilon(\mathbf{k}_{\parallel}) = M_0 - 2[B_2(2 - \cos k_x a - \cos k_y a) + B_1]/a^2$ . Within this model the eigenstates are again helicity degenerate (with the helicity operator properly extended to the discrete case) but this degeneracy is broken when an electric field along the  $z$  direction,  $\hat{V}_{ij} = 2V(i - (N_z + 1)/2)/(N_z - 1)\delta_{ij}$ , is introduced.

To include the effect of induced pairing correlations on the film we consider the Bogoliubov de Gennes (BdG) Hamiltonian, expressed in the basis  $\Psi_j^{\dagger}(\mathbf{k}_{\parallel}) = (\psi_{k_{\parallel}, j}, -i\sigma_y \psi_{-k_{\parallel}, j})$ . It reads

$$\hat{\mathcal{H}}^{BdG}(k_{\parallel})_{ij} = \left( \hat{\mathcal{H}}(\mathbf{k}_{\parallel})_{ij} + \hat{V}_{ij} - \mu \right) \otimes \eta_z + \hat{\Delta}_{ij} \otimes \eta_x, \quad (3)$$

where  $\mu$  is the chemical potential, and  $\eta_j$  are Pauli matrices in the particle-hole space. Although this model allows for more general configurations we shall focus in this work in the case depicted in Fig. 1(b), where pairing is induced on the  $i = 1$  layer only, i.e.  $\hat{\Delta}_{ij} = \hat{\Delta}_1 \delta_{i1} \delta_{ij}$ .  $\hat{\Delta}_1$  has *intra* ( $\Delta_{\pm}$ ) and *inter* ( $\Lambda$ ) parity components,

$$\hat{\Delta}_1 = \frac{\Delta_+}{2} (\tau_0 + \tau_z) + \frac{\Delta_-}{2} (\tau_0 - \tau_z) + \Lambda \tau_x. \quad (4)$$

The pairing potentials depend on the coupling of the TI with the superconductor underneath. As discussed in the SM [41], they would typically have the form  $\Delta_{\pm} = \pi \rho_F t_{\pm}^2$  and  $\Lambda = \pi t_+ t_- \rho_F$ , where  $\rho_F$  is the superconductor Fermi level density of states and  $t_{\pm}$  are hopping parameters coupling the TI orbitals with parity  $\pm$  and the superconductor. These parameters may have opposite signs. In particular, when the ordinary superconductor is contacted to the bottom of the film one expects  $t_+ t_- < 0$ , which implies that  $\Lambda$  has an overall sign with respect to  $\Delta_{\pm}$ . On the contrary, when the superconductor is contacted to the top surface,  $t_+ t_- > 0$  and thus  $\Delta_{\pm}$  and  $\Lambda$  have the same sign.

It should be stressed that the above expressions are fully compatible with time-reversal symmetry. Regarding the size of  $\Lambda$ , while a non-interacting model suggests  $\Lambda \sim \sqrt{\Delta_+ \Delta_-}$ , the presence of moderate local Coulomb repulsion on the Bi and Se sites would yield the condition  $\Lambda > \sqrt{\Delta_+ \Delta_-}$  which is necessary for stabilizing the DIII-TS phase as we show below.

### III. TOPOLOGICAL INVARIANT

In the limit of weak coupling, the topological character of the proximitized TI film can be fully determined by the normal electronic properties at the Fermi level [44]. The  $Z_2$  topological invariant introduced in Ref. [44] is given by

$$N = \prod_n \left( \text{sign} \langle \psi_n(k_{F,n}) | \mathcal{T} \hat{\Delta}^\dagger | \psi_n(k_{F,n}) \rangle \right)^{m_n}, \quad (5)$$

where  $\mathcal{T} = \tau_0 \otimes i\sigma_y K$  with  $K$  denoting complex conjugation, is the time-reversal operator,  $n$  runs over all bands crossing the Fermi energy,  $m_n$  is the number of TRI points enclosed by a band  $n$  and  $|\psi_n(k_{F,n})\rangle$  is the eigenstate on band  $n$  at the Fermi surface. In TIs of the  $\text{Bi}_2\text{Se}_3$  family the only TRI point enclosed by the surface bands is the  $\Gamma$  point so that  $m_n = 1$ . On the other hand, due to the gap isotropy Eq. (5) can be evaluated along any direction in the  $k_x - k_y$  plane.

As a paradigmatic example we shall examine the case  $N_z = 2$ . Details on the calculations are presented in the SM [41], where we also discuss the peculiar  $N_z = 1$  case. The spectrum for  $N_z = 2$  consists of four bands with positive energy which, expanded in  $\mathbf{k} \equiv \mathbf{k}_\parallel$ , are given by

$$E_{\alpha,\chi}(k) = \sqrt{E_1^2 + 2\alpha F_\chi + A_\chi^2 + V^2}. \quad (6)$$

$\alpha = \pm 1$  is a band index,  $E_1^2 = \epsilon_k^2 + A^2 k^2 + B^2 + C^2$ ,  $F_\chi = \sqrt{(BC - \chi A_2 |k| V)^2 + \epsilon_k^2 (V^2 + B^2)}$ ,  $\epsilon_k = M_0 - 2B_1/a^2 + B_2 k^2$ , with  $k = |\mathbf{k}|$  and we have defined the parameters as  $A = A_1/a$ ,  $B = B_1/a^2$  and  $C = A_2/2a$ . The bands and their evolution with voltage  $V$  are shown in Fig 1(a). We focus on a chemical potential  $\mu$  as indicated in Fig. 1(a), intersecting the bands with  $\alpha = -1$ . A non-trivial value of the  $Z_2$  invariant in the present case (i.e.  $N = -1$ ) implies simply different signs of the projected pairing in the two helicity channels,

$$\langle \psi_\chi | \mathcal{T} \hat{\Delta}^\dagger | \psi_\chi \rangle = 2|D_+|^2 (\Delta_+ + \Delta_- \pi_\chi^2) (1 - \beta_\chi \Lambda). \quad (7)$$

In this expression we have introduced the quantities  $D_+$ ,  $\pi_\chi = D_-/D_+$  and  $\beta_\chi = 2\pi_\chi/(\Delta_+ + \Delta_- \pi_\chi^2)$ , which are defined from the components of the eigenstates of  $\hat{H}^{TB}$  on the bottom surface, i.e. we have  $|\psi_\chi\rangle = (\hat{D}_\chi, \hat{U}_\chi)^T$ , where  $\hat{U}_\chi = (U_+, U_-)^T \otimes \hat{\phi}_\chi$  and  $\hat{D}_\chi = (D_+, D_-)^T \otimes \hat{\phi}_\chi$ , and  $\hat{\phi}_\chi$  are the eigenstates of the helicity operator, so

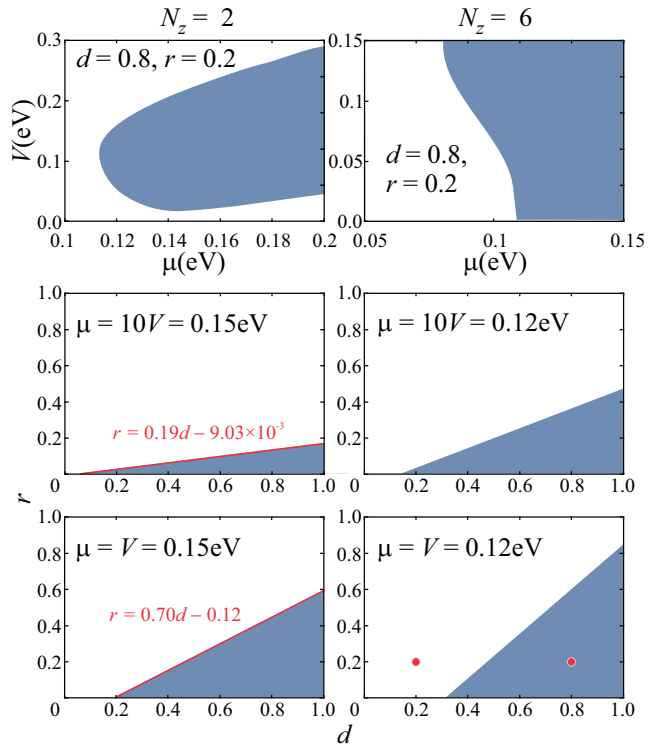


Figure 2: Phase diagrams in the  $V, \mu$  plane at fixed  $r = 0.2$  and  $d = 0.8$  (upper panels) and in the  $r = \Delta_+/\Delta_-$ ,  $d = \Lambda/\Delta_-$  plane at fixed  $\mu = 10V$  (middle panels) and at  $\mu = V$  (lower panels) for the cases  $N_z = 2$  and  $N_z = 6$ . The dark (white) color indicates the topological (trivial) regions. As can be observed, larger values of  $V$  help to stabilize the topological phase for in a broader parameter region. The red lines in the  $d-r$  diagrams for the  $N_z = 2$  case are the analytical prediction for the phase boundary as described in the SM [41].

that  $\phi_\chi$  measures the relative weight of the two parity sector components on the bottom surface. We then see that for having a non-trivial value of the  $Z_2$  topological invariant, the necessary (however not sufficient) condition is  $\pi_\chi$  (or equivalently  $\beta_\chi$ ) having different signs for the two helicities. An analytic expression for  $\pi_\chi$  is given in [41].

As can be observed in Fig. 1(a), the  $\pi_\chi$  parameter evolves differently along the lowest bands with opposite helicities, which are split due to the action of the electric field. While it remains negative for the  $\chi = -1$  band for all values of the chemical potential within the TI gap, in the  $\chi = +1$  band it evolves from negative to positive above a certain critical value of the momentum. As a consequence, for a chemical potential within this energy range and depending on the bias potential  $V$ , the effective pairing of Eq. (24) may have different signs on the two helicity bands leading to a non-trivial value of the  $Z_2$  invariant, provided that, in addition,  $\beta_+ > 1/\Lambda$ . (see SM [41] for further details). In the following we study the occurrence of the TS phase as a function of the parameters  $r = \Delta_+/\Delta_-$  and  $d = \Lambda/\Delta_-$  which determine the relative

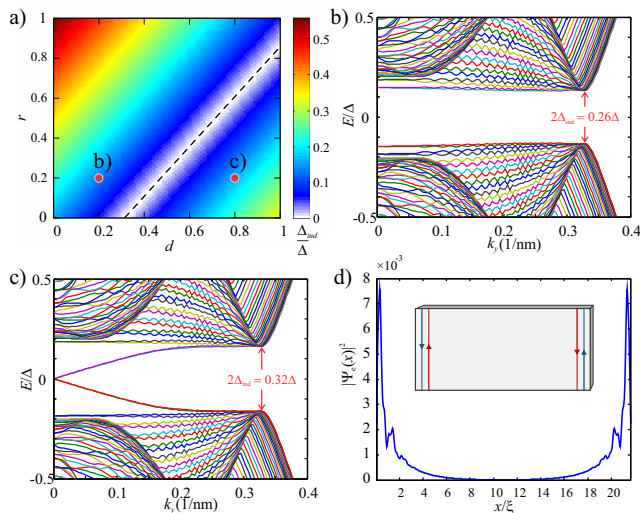


Figure 3: a) Induced gap  $\Delta_{ind}$  in the  $(d, r)$  plane for the same parameters as in the lower right panel of Fig. 2. b-c) BdG spectrum for a slab of finite width  $W \sim 20\xi$ , where  $\xi \sim A_2/\Delta$  is the coherence length in the TI film for the cases indicated by the red dots in panel a). As can be observed, subgap states reaching zero energy for  $k_y \rightarrow 0$  appear in the topological case. b) Electron probability amplitude for these zero energy states.

size of the intra and interparity pairing. We take  $\Delta = \Delta_-$  as the reference energy.

In the Fig. 2 we show the phase diagrams in the  $(\mu, V)$  and in the  $(d, r)$  planes for the  $N_z = 2$  and  $N_z = 6$  cases. As can be observed in the upper panels, the topological phase appears for  $\mu$  above a certain value which decreases for increasing  $N_z$ , corresponding to the closing of the hybridization gap between the surface states. On the other hand  $\mu$  should not exceed a value  $\sim 0.25eV$  where higher bands start to be populated. In addition we observe that a finite  $V$  is needed in order to extend the stability of the topological phase in the  $(d, r)$  plane. For small  $V$  values (middle panels in Fig. 2) the stability is restricted to the regions  $d \rightarrow 1$  and  $r \rightarrow 0$  but these regions grow when  $V \sim \mu$ , gradually reaching the optimal case where the TS phase appears for  $\Lambda > \sqrt{\Delta_+ \Delta_-}$ .

Another important aspect of the proximity effect in the TI film is the size of the induced gap parameter  $\Delta_{ind}$ , which is determined by the smaller value of  $|\langle \psi_\chi | \mathcal{T} \hat{\Delta}^\dagger | \psi_\chi \rangle|$  at the Fermi surface. As shown in Fig. 3(a) this quantity drops to zero at the boundary between the trivial and the TS region at the  $(d, r)$  plane, as expected for a topological transition, and increases when departing from this boundary. The size of  $\Delta_{ind}$  can be more clearly appreciated in Figs. 3(b,c) where we show the BdG spectrum for a  $N_z = 6$  film of finite width in the  $x$  direction. The two cases correspond to parameters within the trivial and the topological regions, as indicated by the two dots in the lower right panel of Fig. 2 and in Fig. 3(a). In the former case the spectrum ex-

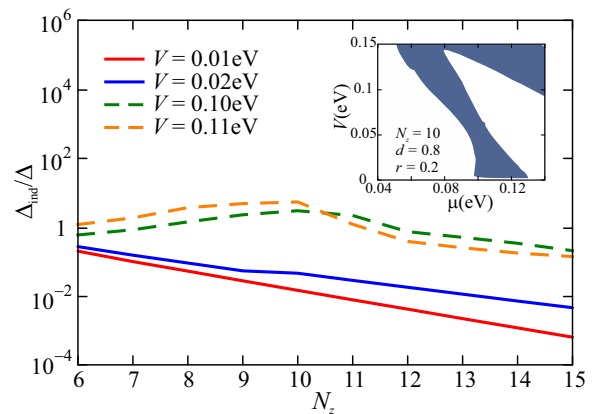


Figure 4: Induced gap as a function of the TI layer thickness ( $N_z$ ) for fixed  $\mu = 0.04eV$  and different values of  $V$ . Full and dashed lines indicate trivial and topological phases respectively. The relative weight of the inter and intra parity pairing at the bottom layer was fixed to  $d = 0.8$  and  $r = 0.2$ . The inset shows the phase diagram in the  $\mu$ - $V$  plane for  $N_z = 10$ .

hibits a pair subgap states, dropping to zero energy for  $k_y \rightarrow 0$ . The corresponding wavefunction, exhibiting localization at the edges of the film, is plotted in Fig. 3(d). Notice that the localization length is of the order of  $5\xi$ , which coincides with an effective coherence length  $\xi_{eff} \sim A_2/\Delta_{ind}$ . As expected for a TS-DIII phase, these states correspond to Kramers pairs of Majorana modes.

The above results correspond to very thin TI layers with  $N_z \leq 6$ . When  $N_z$  is further increased the DIII-TS phase can still be reached for certain parameters values, but the topological region shrinks and the phase diagram starts to exhibit disconnected regions, as shown in the inset of Fig. 4 for  $N_z = 10$ . The behavior of the induced gap with  $N_z$  depends on the  $V$  value. While for small  $V$  values, i.e., outside the topological region, it decreases exponentially with  $N_z$ ; for larger  $V$  it exhibits a non-monotonic behavior, first increasing and eventually decreasing for  $N_z \geq 10$ , as can be observed in the main frame of Fig. 4. This behavior is associated to the fact that higher bands start to cross the chemical potential.

A word of caution is in order regarding the reliability of the precise quantitative predictions of our model, which can nevertheless be trusted at a qualitative level. It is also important to remark that when the film is contacted to a superconductor through both surfaces, thus recovering the inversion symmetry, the topological phase disappears [41].

#### IV. CONCLUSIONS

We have shown that a time reversal invariant TS phase can be induced on a TI film of the  $Bi_2Se_3$  family proximitized by a conventional superconductor. In contrast to previous proposals our mechanism does not rely on tuning the phase difference in a S/TI/S junction but

arises from the induced interparity pairing which naturally occurs at the S/TI interface. The mechanism requires breaking the spatial inversion symmetry and a certain degree of hybridization between the TI surface states. Application of an electric field perpendicular to the layers helps to stabilize the TS phase for thicker films in a broader parameter space. Notice that such fields appear spontaneously at the interface between a TI film and its substrate due to charge accumulation [38].

As a final remark let us mention that proximitized  $\text{Bi}_2\text{Se}_3$  films have been analyzed in several experiments, either through Josephson effect [45, 46] or by tunnel spec-

troscopy [47, 48]. We hope that our work could motivate further experimental studies on this type of devices.

*Acknowledgments:* We thank L. Brey and J. Schmalian for useful comments on the manuscript. This work has been supported by Spanish MINECO through Grants No. FIS2014-55486-P, FIS2017-84860-R and through the “María de Maeztu” Programme for Units of Excellence in R&D (MDM-2014-0377). LA thanks support from CONICET and SECyT from Argentina, as well as the Alexander von Humboldt foundation from Germany. WJH and OEC acknowledge funding from COLCIENCIAS, project No. 110165843163 and doctorate Scholarship 617.

- 
- [1] M. Sato and Y. Ando, Topological Superconductors: a review. *Rep. Prog. Phys.* **80**, 076501 (2017).
- [2] S. Vijay, T. H. Hsieh and L. Fu, Majorana Fermion Surface Code for Universal Quantum Computation, *Phys. Rev. X* **5**, 041038 (2015); S. Plugge, A. Rasmussen, R. Egger and K. Flensberg, Majorana Box Qubits, *New J. Phys.* **19**, 012001 (2017).
- [3] A. P. Mackenzie and Y. Maeno, The superconductivity of  $\text{Sr}_2\text{RuO}_4$  and the physics of spin-triplet pairing, *Rev. Mod. Phys.* **75**, 657 (2003).
- [4] V. Mourik, K. Zuo, S. M. Frolov, S. R. Plissard, E. P. a. M. Bakkers, and L. P. Kouwenhoven, Signatures of Majorana fermions in in hybrid superconductor-semiconductor nanowire devices, *Science* **336**, 1003 (2012).
- [5] A. Das, Y. Ronen, Y. Most, Y. Oreg, M. Heiblum, and H. Shtrikman, Zero-bias peaks and splitting in an Al-InAs nanowire topological superconductor as a signature of Majorana fermions, *Nat. Phys.* **8**, 887 (2012).
- [6] S. M. Albrecht, A. P. Higginbotham, M. Madsen, F. Kuemmeth, T. S. Jespersen, J. Nyg, P. Krogstrup, and C. M. Marcus, Exponential protection of zero modes in Majorana islands, *Nature* **531**, 206 (2016).
- [7] M. Deng, S. Vaitiekenas, E. Hansen, J. Danon, M. Leijnse, K. Flensberg, J. Nygard, P. Krogstrup, and C. Marcus, Majorana bound state in a coupled quantum-dot hybrid-nanowire system, *Science* **354**, 1557 (2016).
- [8] H. J. Suominen, M. Kjaergaard, A. R. Hamilton, J. Shabani, C. J. Palmstrm, C. M. Marcus, and F. Nichele, Scalable Majorana Devices, *Phys. Rev. Lett.* **119**, 176805 (2017).
- [9] S. Nadj-Perge, I.K. Drozdov, J. Li, H. Chen, S. Jeon, J. Seo, A. H. MacDonald, B. A. Bernevig, and A. Yazdani, Topological matter. Observation of Majorana fermions in ferromagnetic atomic chains on a superconductor, *Science* **346**, 602 (2014).
- [10] For a recent review see A. Haim and Y. Oreg, Time Reversal-Invariant Topological Superconductivity, *cond-mat* 1809.06863.
- [11] K. Wölms, A. Stern, and K. Flensberg, Local Adiabatic Mixing of Kramers Pairs of Majorana Bound States, *Phys. Rev. Lett.* **113**, 246401 (2014).
- [12] K. Wölms, A. Stern, and K. Flensberg, Braiding properties of Majorana Kramers pairs, *Phys. Rev. B* **93**, 045417 (2016).
- [13] J. Li, W. Pan, B.A. Bernevig, R.M. Lutchyn, Detection of Majorana Kramers pairs using a quantum point contact *Phys. Rev. Lett.* **117**, 046804 (2016).
- [14] C. Schrade, L. Fu, Parity-controlled  $2\pi$  Josephson effect mediated by Majorana Kramers pairs, *Phys. Rev. Lett.* **120**, 267002 (2018).
- [15] A. Keselman, L. Fu, A. Stern, and E. Berg, Inducing Time-Reversal-Invariant Topological Superconductivity and Fermion Parity Pumping in Quantum Wires, *Phys. Rev. Lett.* **111**, 116402 (2013).
- [16] A. Camjayi, L. Arrachea, A. Aligia and F. von Oppen, Fractional Spin and Josephson Effect in Time-Reversal-Invariant Topological Superconductors, *Phys. Rev. Lett.* **119**, 046801 (2017).
- [17] M. Mashkooi, A. G. Moghaddam, M. H. Hajibabae, A. M. Black-Schaffer, F. Parhizgar, Impact of topology on the impurity effects in extended s-wave superconductors with spin-orbit coupling, arXiv:1805.11885.
- [18] A. Aligia and L. Arrachea, Entangled end states with fractionalized spin projection in a time-reversal-invariant topological superconducting wire, arXiv:1806.06104.
- [19] X.-L. Qi, T.L. Hughes, S. Raghu, and S.-C. Zhang, Time-Reversal-Invariant Topological Superconductors and Superfluids in Two and Three Dimensions, *Phys. Rev. Lett.* **102**, 187001 (2009).
- [20] L. Fu and E. Berg, Odd-parity topological superconductors: Theory and application to  $\text{Cu}_x\text{Bi}_2\text{Se}_3$ , *Phys. Rev. Lett.* **105**, 097001 (2010).
- [21] Ma. S. Scheurer and J. Schmalian, Topological superconductivity and unconventional pairing in oxide interfaces, *Nature Comm.* **6**, 6005 (2015).
- [22] A. Haim, E. Berg, K. Flensberg, Y. Oreg, No-go theorem for a time-reversal invariant topological phase in noninteracting systems coupled to conventional superconductors, *Phys. Rev. B* **94**, 161110 (2016).
- [23] C. L. M. Wong and K. T. Law, Majorana Kramers doublets in  $d_{x^2-y^2}$ -wave superconductors with Rashba spin-orbit coupling *Phys. Rev. B* **86**, 184516 (2012).
- [24] F. Zhang, C. L. Kane, and E. J. Mele, Time-Reversal-Invariant Topological Superconductivity and Majorana Kramers Pairs *Phys. Rev. Lett.* **111**, 056402 (2013).
- [25] E. Gaidamauskas, J. Paaske, and K. Flensberg, Majorana Bound States in Two-Channel Time-Reversal-Symmetric Nanowire System, *Phys. Rev. Lett.* **112**, 126402 (2014).
- [26] J. Klinovaja, A. Yacoby, and D. Loss, Kramers pairs of Majorana fermions and parafermions in fractional topological insulators, *Phys. Rev. B* **90**, 155447 (2014).
- [27] H. Ebisu, B. Lu, J. Klinovaja and Y. Tanaka, The-

- ory of time-reversal topological superconductivity in double Rashba wires: symmetries of Cooper pairs and Andreev bound states, *Prog. Theor. Exp. Phys.* **2016**, 083I01 (2016).
- [28] C. Reeg, C. Schrade, J. Klinovaja, D. Loss, DIII Topological Superconductivity with Emergent Time-Reversal Symmetry, *Phys. Rev. B* **96**, 161407 (2017).
- [29] Arbel Haim, Anna Keselman, Erez Berg, Yuval Oreg, Time-Reversal Invariant Topological Superconductivity Induced by Repulsive Interactions in Quantum Wires, *Phys. Rev. B* **89**, 220504(R) (2014).
- [30] Arbel Haim, Konrad Wölms, Erez Berg, Yuval Oreg, Karsten Flensberg, Interaction-driven topological superconductivity in one dimension, *Phys. Rev. B* **94**, 115124 (2016).
- [31] L. Fu and C. Kane, Superconducting proximity effect and majorana fermions at the surface of a topological insulator, *Phys. Rev. Lett.* **100**, 096407 (2008).
- [32] L. Santos, T. Neupert, C. Chamon and C. Mudry, Superconductivity on the surface of topological insulators and in two-dimensional noncentrosymmetric materials, *Phys. Rev. B* **81**, 184502 (2010).
- [33] C.-X. Liu Tand B. Trauzettel, Helical Dirac-Majorana interferometer in a superconductor/topological insulator sandwich structure, *Phys. Rev. B* **83**, 220510 (2011).
- [34] C. Schrade, A.A. Zyuzin, J. Klinovaja, and Daniel Loss, Proximity-Induced  $\pi$  Josephson Junctions in Topological Insulators and Kramers Pairs of Majorana Fermions, *Phys. Rev. Lett.* **115**, 237001 (2015).
- [35] F. Parhizgar and A. M. Black-Schaffer, Highly tunable time-reversal-invariant topological superconductivity in topological insulator thin films, *Scientific Reports* **7**, 9817 (2017).
- [36] H. Zhang, C.-X. Liu, X.-L. Qi, X. Dai, Z. Fang and S.-C. Zhang, Topological insulators in  $\text{Bi}_2\text{Se}_3, \text{Bi}_2\text{Te}_3$  and  $\text{Sb}_2\text{Te}_3$  with a single Dirac cone on the surface, *Nature Phys.* **5**, 438 (2009).
- [37] C.-X. Liu, X.-L. Qi, H. Zhang, X. Dai, Z. Fang, and S.-C. Zhang, Model hamiltonian for topological insulators, *Phys. Rev. B* **82**, 045122 (2010).
- [38] Y. Zhang et al., Crossover of the three-dimensional topological insulator  $\text{Bi}_2\Delta\text{Se}\Delta_3$  to the two-dimensional limit, *Nature Phys.* **6**, 584 (2010).
- [39] H.-Z. Lu, W.-Yu Shan, W. Yao, Q. Niu and S.-Q. Shen, Massive Dirac fermions and spin physics in an ultrathin film of topological insulator, *Phys. Rev. B* **81**, 115407 (2010).
- [40] P. G. Silvestrov, P. W. Brouwer, and E. G. Mishchenko, Spin and charge structure of the surface states in topological insulators, *Phys. Rev. B* **86**, 075302 (2012).
- [41] Supplementary Information.
- [42] According to Ref. [37] appropriate parameters for  $\text{Bi}_2\text{Se}_3$ , obtained from fits to *ab initio* calculations are  $M_0 = 0.28$  eV,  $A_1 = 2.26$  eVÅ,  $A_2 = 3.33$  eVÅ,  $B_1 = 6.86$  eVÅ<sup>2</sup> and  $B_2 = 44.5$  eVÅ<sup>2</sup>.
- [43] S. Acero, L. Brey, W.J. Herrera, and A. Levy Yeyati, Transport in selectively magnetically doped topological insulator wires, *Phys. Rev. B* **92**, 235445 (2015).
- [44] X.-L. Qi, T. L. Hughes, and S.-C. Zhang, Topological invariants for the fermi surface of a time-reversal-invariant superconductor, *Phys. Rev. B* **81**, 134508 (2010).
- [45] J. R. Williams et al., Unconventional Josephson effect in hybrid superconductor-topological insulator devices, *Phys. Rev. Lett.* **109**, 056803 (2012).
- [46] M. Snelder, C.G. Molenaar, Y. Pan, D. Wu, Y. K. Huang, A. de Visser, A. A. Golubov, W.G. van der Wiel, H. Hilgenkamp, M.S. Golden and A. Brinkman, Josephson supercurrent in a topological insulator without a bulk shunt. *Supercond. Sci. Technol.* **27**, 104001 (2014).
- [47] F. Yang et al., Proximity-effect-induced superconducting phase in the topological insulator  $\text{Bi}_2\text{Se}_3$ . *Phys. Rev. B* **86**, 134504 (2012).
- [48] A. Finck, C. Kurter, Y. Hor and D. Van Harlingen, Phase coherence and Andreev reflection in topological insulator devices. *Phys. Rev. X* **4**, 041022 (2014).

## V. SUPPLEMENTAL MATERIAL

### A. Unitary transformation on the k-p model of Ref. [1]

According to Ref. [1] the low-energy and long-wavelength electronic properties of  $\text{Bi}_2\text{Se}_3$  can be described by a Hamiltonian written in a basis of four states which are combinations of  $p_z$  orbitals of Bi and Se with even and odd parities given by

$$\tilde{H}^{3D} = \mathcal{M}(\mathbf{k})\tau_z \otimes \sigma_0 + A_1 k_z \tau_x \otimes \sigma_z + A_2 (k_x \sigma_x + k_y \sigma_y) \otimes \tau_x, \quad (8)$$

where  $\mathcal{M}(\mathbf{k}) = M_0 - B_1 k_x^2 - B_2 (k_x^2 + k_y^2)$  and  $\tau_\alpha$  and  $\sigma_\alpha$  are Pauli matrices operating in different pseudospin spaces. While matrices  $\tau_\alpha$  refer to the  $P1_z^+$  and  $P2_z^-$  orbitals which are mainly located on the Bi and Se sublattices respectively [1], the  $\sigma_\alpha$  matrices do not correspond exactly to the *real* spin but are related to it by [2]

$$s_x = \tau_z \otimes \sigma_x, \quad s_y = \tau_z \otimes \sigma_y, \quad s_z = \tau_0 \otimes \sigma_z. \quad (9)$$

For analyzing proximity induced superconductivity it is convenient to write the system Hamiltonian in a basis where the  $\sigma_\alpha$  matrices correspond to the real spin. For this purpose one can perform the following unitary transformation [2]

$$U = \frac{\tau_0 + \tau_z}{2} + i(\sigma \cdot \mathbf{n}) \frac{\tau_0 - \tau_z}{2}, \quad (10)$$

where  $\mathbf{n}$  is a unitary vector along the  $c$  axis. Applying this transformation to Hamiltonian (8) for  $\mathbf{n} = +\hat{z}$  one obtains the model given in Eq. (1) of the main text.

### B. Origin of intra and inter parity pairing

The description of the superconducting proximity effect used in this work can be considered as the low-energy theory arising from integrating out the degrees of freedom of the proximitized superconductor in the Green's function formalism. After this integration the proximity effect is encoded in a self-energy [3]

$$\hat{\Sigma}_{\tau,\tau'}(\omega) = \hat{t}_\tau \hat{g}(\omega) \hat{t}_{\tau'}, \quad (11)$$

where  $\hat{t}_\tau = t_\tau \eta_z \sigma_0$ , where  $t_\tau$  are the hopping amplitudes from the SC to the  $\tau$  parity orbitals on the first layer of the TI,  $\eta_j$  denote the Pauli matrices in particle-hole space, and  $\hat{g}(\omega)$  is the superconductor Green function, which for the BCS case is given by

$$\hat{g}(\omega) = \pi \rho_F \frac{-\omega + \Delta_0 \eta_x}{\sqrt{\Delta_0^2 - \omega^2}} \sigma_0, \quad (12)$$

where  $\Delta_0$  is the pairing potential of the parent superconductor and  $\rho_F$  denotes its Fermi level density of states. The parameters  $\Delta_\pm$  and  $\Lambda$  in the main text thus arise from the elements  $\Sigma_{\tau,\tau'}^{e,h}$  in the limit  $\omega \rightarrow 0$ .

### C. Limit $N_z = 1$

The aim of this section is to show that the model we are considering contains the ingredients for topological superconductivity even in the extreme limit of a single monolayer in proximity to an ordinary superconductor.

We consider the Hamiltonian of Eq. (2) of the main text with  $N_z = 1$

$$\hat{\mathcal{H}}_1 = \epsilon(\mathbf{k}_\parallel) \tau_z + a_2 \tau_x \otimes [\sin(k_y a) \sigma_x - \sin(k_x a) \sigma_y], \quad (13)$$

where we have defined  $a_2 = A_2/a$ . We introduce the Nambu spinor  $\Psi^\dagger(\mathbf{k}_\parallel) = (\psi^\dagger(\mathbf{k}_\parallel), -i\sigma_y \psi(-\mathbf{k}_\parallel))$ , where  $\psi(\mathbf{k}_\parallel)$  is a spinor of the basis of  $\hat{\mathcal{H}}_1$ .

The matrix for the Bogoliubov de Gennes Hamiltonian of the monolayer of the Hamiltonian of Eq. (3) of the main text with induced superconductivity reads

$$\begin{aligned} \hat{\mathcal{H}}_1^{BdG} &= \left( \hat{\mathcal{H}}_1 - \mu \right) \otimes \eta_z + \\ &+ \left[ \frac{\Delta_+}{2} (\tau_0 + \tau_z) + \frac{\Delta_-}{2} (\tau_0 - \tau_z) + \Lambda \tau_x \right] \otimes \eta_x. \end{aligned} \quad (14)$$

We can now introduce a rotation with respect to the  $y$  axis in the parity space such that  $\tau_x \rightarrow -\tilde{\tau}_z$  and  $\tau_z \rightarrow \tilde{\tau}_x$  and focus on the case with  $\Delta_+ = \Delta_- = 0$ . The resulting Hamiltonian reads

$$\begin{aligned} \hat{\mathcal{H}}_1^{BdG} &= \eta_z \otimes (\epsilon(\mathbf{k}_\parallel) \tilde{\tau}_x - \mu \tau_0) - \Lambda (\eta_x \otimes \tilde{\tau}_z) \\ &- a_2 \tilde{\tau}_z \otimes [\sin(k_y a) \sigma_x - \sin(k_x a) \sigma_y] \otimes \eta_z \end{aligned} \quad (15)$$

We see that along the directions  $(k_x, 0)$  and  $(k_y, 0)$  this Hamiltonian has an identical structure as the 1D model ladder model introduced by Keselman et al in Ref. 4, upon identifying the two parity projections  $e, o$  (even, odd) with the two legs of the ladder Hamiltonian of that paper. Importantly, the Hamiltonian of Eq. (15) has different signs of the pairing and of the spin orbit interaction in the two different parity channels of the rotated basis. Therefore, we know from Ref. 4 that it hosts a topological phase.

### D. Model and symmetries for $N_z = 2$

Here we consider the case  $N_z = 2$ , for which we can obtain some analytical results, specially for the  $\mathbb{Z}_2$  topological invariant. The two layers are labeled with the indices  $U$  (up) and  $D$  (down). The matrix for the model Hamiltonian can be written as follows

$$\begin{aligned} \hat{\mathcal{H}}_2 &= \epsilon(\mathbf{k}_\parallel) f_0 \otimes \tau_z \otimes \sigma_0 + A_2 f_0 \otimes \tau_x \otimes k_\parallel \hat{h} \\ &+ B f_x \otimes \tau_z \otimes \sigma_0 + C f_y \otimes \tau_y \otimes \sigma_0 \\ &- V f_z \otimes \tau_0 \otimes \sigma_0, \end{aligned} \quad (16)$$

where  $B = B_1/a^2$ ,  $C = A_1/2a$ ,  $f_i$  are Pauli matrices in the surface space, and  $\epsilon = M_0 - 2B_1/a^2 - B_2 |\mathbf{k}|^2$ , while  $V$  is the scalar potential, representing a potential difference of  $2V$  between the opposite surfaces of the film.

We introduce the discretized version of the helicity operator  $\Xi = f_0 \otimes \tau_0 \otimes \hat{h}$ . The Hamiltonian (16) commutes with this operator,  $[\Xi, \hat{\mathcal{H}}_2] = 0$ . Thus, the states can be labeled with  $\chi = \pm$ , which correspond to the two eigenstates of the helicity operator  $\hat{h}$ ,  $\hat{\phi}_\chi(\mathbf{k}_\parallel) = (i\chi, e^{i\theta})^T / \sqrt{2}$ , with  $e^{i\theta} = (k_x + ik_y) / k_\parallel$ .

The Hamiltonian (16) is time-reversal invariant, i.e.  $\mathcal{T} \hat{\mathcal{H}}(\mathbf{k}_\parallel) \mathcal{T}^{-1} = \hat{\mathcal{H}}(-\mathbf{k}_\parallel)$ . For  $V = 0$  it also has inversion symmetry  $\mathcal{P} \hat{\mathcal{H}}(\mathbf{k}_\parallel) \mathcal{P} = \hat{\mathcal{H}}(-\mathbf{k}_\parallel)$  with  $\mathcal{P} = f_x \otimes \tau_z \otimes \sigma_0$ . Therefore, the eigenstates with eigenenergies  $E_{n,\mathbf{k}_\parallel,\chi}$  satisfy the following properties

$$\mathcal{T} \psi_{n,\mathbf{k}_\parallel,\chi} = \psi_{n',-\mathbf{k}_\parallel,\chi}, \quad (17)$$

$$E_{n,\mathbf{k}_\parallel,\chi} = E_{n',-\mathbf{k}_\parallel,\chi}, \quad (18)$$

and for  $V = 0$

$$\mathcal{P} \psi_{n,\mathbf{k}_\parallel,\chi} = \psi_{n,-\mathbf{k}_\parallel,-\chi}, \quad (19)$$

$$E_{n,\mathbf{k}_\parallel,\chi} = E_{n,-\mathbf{k}_\parallel,-\chi}. \quad (20)$$

We also consider the Bogoliubov de Gennes Hamiltonian for the bilayer system in proximity to superconductors in the most general case, where the induced pairing potential has different amplitudes in the two layers,  $\hat{\Delta}^{U,D}$ ,  $\hat{\Lambda}^{U,D}$ . The corresponding matrix reads

$$\hat{\mathcal{H}}_2^{BdG} = \mathcal{H}_2 \otimes \eta_z + \mathcal{H}_\Delta, \quad (21)$$

with

$$\mathcal{H}_\Delta = \eta_x \otimes \left( \bar{\Delta} + \tilde{\Delta} f_z + [\bar{\Lambda} + \tilde{\Lambda} f_z] \otimes \tau_x \right),$$

where  $\bar{\Delta} = (\hat{\Delta}_U + \hat{\Delta}_D)/2$ ,  $\bar{\Lambda} = (\hat{\Lambda}_U + \hat{\Lambda}_D)/2$  and  $\tilde{\Delta} = (\hat{\Delta}_U - \hat{\Delta}_D)/2$ ,  $\tilde{\Lambda} = (\hat{\Lambda}_U - \hat{\Lambda}_D)/2$ , where the pairings  $\hat{\Delta}^{U,D}$  in the parity basis are given by  $\hat{\Delta}^{U,D} = \Delta_+^{U,D} (\tau_0 + \tau_z)/2 + \Delta_-^{U,D} (\tau_0 - \tau_z)/2$ .

In addition to time-reversal, this model Hamiltonian exhibits charge conjugation,  $\mathcal{C}\hat{\mathcal{H}}_2(\mathbf{k}_{\parallel})\mathcal{C}^{-1} = -\hat{\mathcal{H}}_2(-\mathbf{k}_{\parallel})$  with  $\mathcal{C} = \eta_x \otimes f_0 \otimes \tau_0 \otimes \sigma_0 K$ , and chiral symmetry  $\Pi\hat{\mathcal{H}}_2(\mathbf{k}_{\parallel})\Pi^{-1} = -\hat{\mathcal{H}}_2(\mathbf{k}_{\parallel})$  with  $\Pi = \mathcal{C}\mathcal{T}$ . This means that this system belongs to the Altland-Zirnbauer class DIII. For  $V = 0$  and  $\Delta = \bar{\Delta} = 0$ , it has, in addition, inversion symmetry with  $\mathcal{P} = \eta_0 \otimes f_x \otimes \tau_z \otimes \sigma_0$ .

### E. $\mathbb{Z}_2$ topological invariant

We now consider the Hamiltonian of Eq. (16) and focus on the direction  $\mathbf{k} = (0, k_y)$ . The eigenstates of  $\mathcal{H}_2$  are expressed as  $|\psi_{\chi}\rangle = \left(\hat{D}_{\chi}, \hat{U}_{\chi}\right)^T$ , with  $\hat{U}_{\chi} = (U_+, U_-)^T \otimes \hat{\phi}_{\chi}$  and  $\hat{D}_{\chi} = (D_+, D_-)^T \otimes \hat{\phi}_{\chi}$ . From the equation  $\hat{H}|\psi_{\chi}\rangle = E_{\chi}|\psi_{\chi}\rangle$  we get that the components of the spinor  $D_i, U_i$  are real constants satisfying

$$\pi_{\chi,D} = \frac{D_-}{D_+} \quad (22)$$

$$= \frac{(CA_{\chi} - X_+B)Y + (CA_{\chi} + Y_-B)\Phi}{(BA_{\chi} - X_-C)Y - (BA_{\chi} + Y_-C)\Phi},$$

$$\pi_{\chi,U} = \frac{U_-}{U_+} \quad (23)$$

$$= -\frac{(BA_{\chi} + Y_+C)X - (BA_{\chi} - X_+C)\Phi}{(CA_{\chi} + Y_-B)X + (CA_{\chi} - X_+B)\Phi},$$

where  $A_{\chi} = A_2\chi k$ ,  $Y = A_{\chi}^2 - Y_+Y_-$ ,  $X = A_{\chi}^2 - X_+X_-$ ,  $X_{\pm} = \pm\epsilon(k_y) - E - V$ ,  $Y_{\pm} = \pm\epsilon(k_y) - E + V$ ,  $\Phi = C^2 - B^2$ . The energy bands  $E_{\chi}$  are given by the expressions

$$E_{\alpha,\chi} = \pm\sqrt{E_1^2 + 2\alpha F_{\chi} + A_{\chi}^2 + V^2},$$

$$F_{\chi} = \sqrt{(BC - \chi A_2|k|V)^2 + \epsilon^2(V^2 + B^2)}.$$

Here  $\alpha = \pm$  defines a band index and we have introduced the definition  $E_1^2 = \epsilon^2 + B^2 + C^2$ . Fig.1 (a) of the main text illustrates the behavior of the ratios  $\pi_{\chi}$  for different values of the potential  $V$ . Notice that for  $V = 0$  the bands are degenerate in helicity. In fact, for  $V = 0$  the factor  $F_{\chi}$  and then  $E_{\chi}$  do not depend on  $\chi$ .

We now focus on the superconductivity induced only in the  $D$  surface,  $\hat{\Delta}_D = \hat{\Delta}$ ,  $\hat{\Delta}_U = 0$ ,  $\hat{\Lambda}_D = \hat{\Lambda}$ ,  $\hat{\Lambda}_U = 0$ . This implies  $\bar{\Delta} = -\hat{\Delta} = \Delta/2$ , and  $\bar{\Lambda} = -\hat{\Lambda} = \Lambda/2$  in Eq.(21). By calculating the expectation value of  $\mathcal{T}\hat{\Delta}^{\dagger}$  with the  $D$  surface states we obtain Eq. (7) in the main text, i.e.

$$\begin{aligned} \langle \psi_{\chi} | \mathcal{T}\hat{\Delta}^{\dagger} | \psi_{\chi} \rangle &= 2|D_+|^2 (\Delta_+ + \Delta_- \pi_{\chi}^2 - 2\pi_{\chi}\Lambda) \quad (24) \\ &= 2|D_+|^2 (\Delta_+ + \Delta_- \pi_{\chi}^2) (1 - \beta_{\chi}\Lambda). \end{aligned}$$

Here, we have defined  $\pi_{\chi} \equiv \pi_{\chi,D}(E = \mu)$  as well as the factor

$$\beta_{\chi} = 2\pi_{\chi}/(\Delta_+ + \Delta_- \pi_{\chi}^2). \quad (25)$$

As discussed in the main text, the  $\mathbb{Z}_2$  invariant of Eq. (5) has a non-trivial value when the quantity (24) has different signs for the  $\chi = \pm 1$  bands at the Fermi surface. In turn, a necessary condition is that  $\pi_{\chi}$  has opposite signs for the two helicities. If we have  $\pi_{\bar{\chi}} < 0$  for one band (which warrants  $\langle \psi_{\bar{\chi}} | \mathcal{T}\hat{\Delta}^{\dagger} | \psi_{\bar{\chi}} \rangle > 0$ ) the topological phase may exist in a range of parameters satisfying  $\pi_{\chi} > 0$  and  $\beta_{\chi} > 1/\Lambda$  for the opposite helicity. Notice that  $\pi_{\pm}$  depends only on the intrinsic parameters, as well as on  $\mu$  and  $V$ , while  $\beta_{\pm}$  depends also on the pairing parameters  $\Delta_{\pm}$  and  $\Lambda$ . Hence, the general strategy we follow to define the existence of the topological phase is to identify the range of  $\mu$  and  $V$  for which

$$\beta_{\chi} > 1/\Lambda, \quad \pi_{\chi} > 0, \quad \pi_{\bar{\chi}} < 0. \quad (26)$$

Notice that the maximum value for  $\beta_{\chi}$  occurs for  $\pi_{\chi} = \sqrt{\Delta_+/\Delta_-}$  and corresponds to  $\beta_{\chi} = 1/\sqrt{\Delta_+\Delta_-}$ . In such a case, the change of sign in Eq. (24) occurs for  $\sqrt{\Delta_+\Delta_-} < \Lambda$ .

Interestingly, for  $V = 0$ , there are two limits where Eq. (22) simplifies significantly and we can analytically determine the conditions for a topological phase. (i) For  $C = 0$ , the explicit calculation of the different coefficients casts  $D_+ = 0$ , excluding the possibility of a topological phase. (ii) For  $C = B$  we have

$$\pi_{\chi} = -\frac{A_{\chi} - \epsilon + E}{A_{\chi} + \epsilon + E}, \quad V = 0. \quad (27)$$

Focusing on  $k > 0$ , we see that  $\pi_+ > 0$ , while  $\pi_- < 0$  for  $E - \epsilon < A_2k < E + \epsilon$ . Fixing the chemical potential to satisfy this condition for  $k = k_F$  and  $E = \mu$ , we find the range of  $\mu$  for the topological phase. Then, given a particular  $\mu$  within such range, we can find the conditions to be satisfied for  $\Delta_{\pm}$ ,  $\Lambda$  leading to  $\beta_+ > \Lambda$ .

In the more general case, it is difficult to draw conclusions on the behavior of  $\pi_{\pm}$  on the basis of the analytical expressions, but the procedure is similar than above. Examples are shown in Fig. 5 of this Supplemental Material (SM). In panels (a) and (b) Fig. 5 the behavior of  $\pi_{\pm}$  as a function of  $k_y$  is shown for different values of  $V$ . We see that for most of the cases  $\pi_+ > 0$  (notice that only in the case with  $V = 0.05$  eV this is not satisfied close to  $k_y = 0$ ). Instead  $\pi_-$  shows a discontinuity with a vertical asymptote at  $k_y = k_c$ , which implies a change of sign at  $k_c$ . In panel (b) we focus on  $V = 0.15$  eV and we superimpose the plots of the energy bands. In this way, we can easily identify the portions of the dispersion relation where the conditions  $\pi_+ > 0$  and  $\pi_- < 0$  are simultaneously satisfied for a certain value of the chemical potential  $\mu$ .

Panels (c) and (d) in Fig. 5 correspond to the phase diagram in the space of the pairing parameters  $\Delta_{\pm}$  and  $\Lambda$  for  $\mu = V = 0.15$  eV. The panel (c) corresponds to  $\Delta_+ = \Delta_-$  and the boundary separating the topological and non-topological phases is defined from the conditions of Eq. (26), which in this case is given by

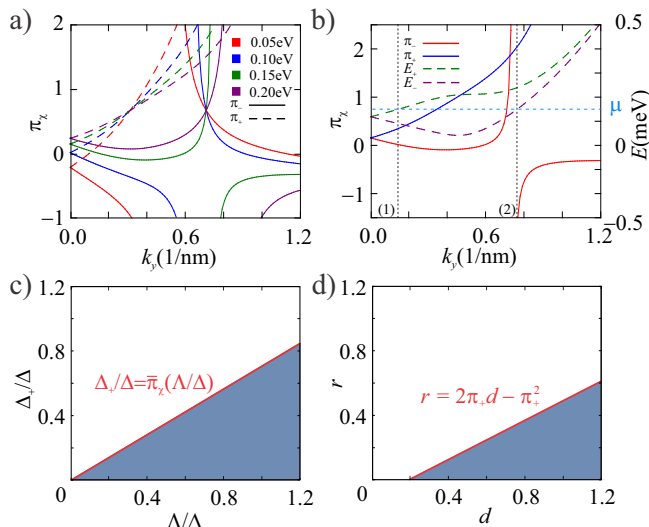


Figure 5: a) Parameters  $\pi_{\chi=\pm}$  in the  $N_z = 2$  case for several  $V$  values as a function of  $k_y$ . Solid lines correspond to  $\pi_-$  and dashed lines to  $\pi_+$ . b) Parameters  $\pi_{\pm}$  (full lines) and energy bands  $E_{-1,\pm}(k_y)$  for the case  $V = 0.15$  eV as a function of  $k_y$ . The vertical dotted lines indicate the Fermi momenta (1) and (2) for the case  $\mu = V$ . c) Phase diagram for the case  $\Delta_+ = \Delta_-$ . The dark (white) color corresponds to the topological (non-topological) phase. d) Same as (c) for the case  $\Delta_- = \text{const}$ .

$\Delta_+ = 2\pi_{\chi}\Lambda/(1+\pi_{\chi}^2) = \bar{\pi}_{\chi}$ . In the panel (b) we illustrate the case with  $\Delta_- = \text{const}$ . As in the main text, we define  $r = \Delta_+/\Delta_-$  and  $d = \Lambda/\Delta_-$ . The boundary between the topological and non-topological phases in this case is given by  $r = 2\pi_{\chi}d - \pi_{\chi}^2$ .

For the pairing only in the up-surface we can repeat the previous analysis by changing  $\pi_{\chi,D} \rightarrow \pi_{\chi,U}$ ,  $\Lambda \rightarrow -\Lambda$ . Finally, in the case of symmetric junction with two identical superconductors contacting the TI film and in the absence of an electric field, the system recovers the inversion symmetry and the topological phase is lost since the contribution to the topological invariant from both surface states has the same sign. While a finite electric field does break this symmetry it does not lead to a robust topological phase, at least for small  $N_z$  values, when both surfaces are contacted to a superconductor.

- [1] C.-X. Liu, X.-L. Qi, H. Zhang, X. Dai, Z. Fang, and S.-C. Zhang, “Model hamiltonian for topological insulators”, Phys. Rev. B **82**, 045122 (2010).  
 [2] P. G. Silvestrov, P. W. Brouwer, and E. G. Mishchenko, “Spin and charge structure of the surface states in topological insulators”, Phys. Rev. B **86**, 075302 (2012).  
 [3] P. Sitthison and T. Stanescu, “Robustness of topological

- superconductivity in proximity-coupled topological insulator nanoribbons”, Phys. Rev. B **90**, 035313 (2014).  
 [4] Anna Keselman, Liang Fu, Ady Stern, Erez Berg, “Inducing time reversal invariant topological superconductivity and fermion parity pumping in quantum wires”, Phys. Rev. Lett. **111**, 116402 (2013)